Application of the dynamic rotational isomeric states model to poly(ethylene oxide) and comparison with nuclear magnetic relaxation data

ARTICLE *in* MACROMOLECULES · SEPTEMBER 1989

Impact Factor: 5.8 · DOI: 10.1021/ma00195a068

3 AUTHORS, INCLUDING:

Ivet Bahar
University of Pittsburgh
305 PUBLICATIONS **12,303** CITATIONS
SEE PROFILE

Burak Erman
Koc University
220 PUBLICATIONS **5,958** CITATIONS
SEE PROFILE

Application of the Dynamic Rotational Isomeric States Model to Poly(ethylene oxide) and Comparison with Nuclear Magnetic Relaxation Data

Ivet Bahar* and Burak Erman

Polymer Research Center, School of Engineering, Bogazici University, Bebek 80815, Istanbul, Turkey

Lucien Monnerie

Laboratoire de Physicochimie Structurale et Macromoleculaire associe au CNRS, E.S.P.C.I., 10 rue Vauquelin, 75231 Paris, France. *Received September 12, 1988; Revised Manuscript Received November 8, 1988*

ABSTRACT: The dynamic rotational isomeric states (RIS) model recently developed for investigating local chain dynamics is further improved and applied to poly(ethylene oxide) (PEO). In general, a set of eigenvalues λ_j, $j = 1$ to ν^N, characterizes the dynamic behavior of a given segment of N motional bonds, with ν isomeric states available to each bond. The eigenvalues may be identified as the frequencies of the individual modes contributing to local chain relaxation. To calculate orientational autocorrelations, time correlations, and/or power spectra, λ_j's are combined with the weighting factors k_j which are determined by the equilibrium statistics of the chain and the specific property investigated. The rates of transitions between isomeric states are assumed to be inversely proportional to solvent viscosity, leading to a linear dependence between viscosity and correlation times. Predictions of the theory are in satisfactory agreement with the isotropic correlation times and spin-lattice relaxation times from ^{13}C and ^1H NMR experiments for PEO in a variety of solvents. An activation energy of about one barrier height is theoretically calculated, in agreement with previous experimental studies.

I. Introduction

In a series of papers,[1-4] local chain dynamics was investigated by using the dynamic rotational isomeric states (RIS) approach based on a model first proposed by Jernigan.[5] The most important advantage of the theory is the fact that real chain characteristics such as the molecular structure and the configurational statistics are incorporated into the calculations. The time dependence of orientational and conformational correlations is accordingly computed for specific vectorial quantities rigidly embedded in short segments of real chains subject to conformational transitions. Calculations performed for polyethylene (PE), the simplest polymeric chain, support the use of the dynamic RIS model as a tool of investigating local chain dynamics. In fact, the stochastics of conformational transitions predicted by the theory are in reasonable agreement with related Brownian[6] simulations. The theoretically obtained decay of the orientational autocorrelation functions (OACF) with time may be fitted[4] to a good approximation by previously proposed functional forms, the Hall-Helfand[7] and Bendler-Yaris[8] expressions, in particular. That an activation energy of about one barrier height (between isomeric states) is associated with conformational transitions in n-alkanes is confirmed[2] by the theory, in agreement with NMR measurement by Matsuo and Stockmayer.[9]

As relatively short segments in motion are considered in the theory due to computational limitations, the theory seems particularly useful for interpreting high frequency relaxations involving correlation times of the order of 10^{-12}-10^{-10} s. Such fast motions are measured in NMR experiments, in particular.

In the present study, the dynamic RIS formulation is improved such that a discrete set of eigenvalues governing the stochastics of conformational transitions is readily obtainable for the specific segment considered. The eigenvalues may be identified with the frequencies of various modes contributing to relaxation. They are used in the calculation of the correlation times, the OACFs, and their Fourier transforms, i.e., the spectral densities.

In the next section, the improved formulation of the dynamic RIS model is presented and the application of the model to poly(ethylene oxide) (PEO) is outlined. Calculations of the OACFs and the spectral densities are illustrated in section III. Predictions of the theory are compared in section IV, with the correlation times and spin-lattice relaxation times measured in ^{13}C NMR and ^1H NMR experiments[10-13] with dilute PEO solutions. The concluding remarks are presented in section V.

II. Theory

Stochastics of Conformational Transitions. The master equation for conformational transitions in a sequence of N skeletal bonds in motion is

$$d\mathbf{P}^{(N)}(t)/dt = \mathbf{A}^{(N)}\mathbf{P}^{(N)}(t) \quad (1)$$

where $\mathbf{P}^{(N)}$ is the column vector of the instantaneous probabilities of the 3^N configurations available in the sequence, on the premises of three states per bond. $\mathbf{A}^{(N)}$ is the $3^N \times 3^N$ transition rate matrix which is constructed according to a suitable kinetic scheme depending on the specific configurational characteristics of the polymer considered. For a sequence in which the simultaneous transitions of two neighboring bonds are correlated, the matrix $\mathbf{A}^{(N)}$ appearing in eq 1 takes the following form:

$$\mathbf{A}^{(N)} = \mathbf{A}^{(2)}_{1,2} \otimes \mathbf{I}_3 \otimes \mathbf{I}_3 \otimes \dots \otimes \mathbf{I}_3 + \mathbf{I}_3 \otimes \mathbf{A}^{(2)}_{2,3} \otimes \mathbf{I}_3 \otimes \dots \otimes \mathbf{I}_3 + \dots + \mathbf{I}_3 \otimes \mathbf{I}_3 \otimes \mathbf{I}_3 \otimes \dots \otimes \mathbf{A}^{(2)}_{N-1,N} = \sum_{j=1}^{N-1} \mathbf{I}_3 \otimes \mathbf{I}_3 \otimes \mathbf{A}^{(2)}_{j,j+1} \otimes \mathbf{I}_3 \otimes \dots \otimes \mathbf{I}_3 \quad (2)$$

Here $\otimes$ indicates the direct product and $\mathbf{A}^{(2)}_{j,j+1}$ is the second-order transition rate matrix for a pair of neighboring bonds whose dynamics are correlated. Further discussion for constructing $\mathbf{A}^{(2)}_{j,j+1}$ for PEO is given below. $\mathbf{I}_3$ is the identity matrix of order 3.

The solution to eq 1 can be written in terms of the eigenvalues and eigenvectors of $\mathbf{A}^{(N)}$ as

$$\mathbf{P}^{(N)}(t) = \boldsymbol{B}^{(N)} \exp\{\boldsymbol{L}^{(N)}t\}[\boldsymbol{B}^{(N)}]^{-1}\mathbf{P}^{(N)}(0) \quad (3)$$

using

$$\mathbf{A}^{(N)}(t) = \boldsymbol{B}^{(N)}\boldsymbol{L}^{(N)}[\boldsymbol{B}^{(N)}]^{-1} \quad (4)$$

where $\boldsymbol{L}^{(N)}$ is the diagonal matrix composed of the ei-

0024-9297/89/2222-2396$01.50/0

genvalues λ_j, $j = 1, 3^N$, of $\mathbf{A}^{(N)}$, and $\boldsymbol{B}^{(N)}$ is the matrix whose jth column is the eigenvector associated with λ_j. $[\boldsymbol{B}^{(N)}]^{-1}$ is the inverse of $\boldsymbol{B}^{(N)}$. It should be noted that one of the eigenvalues, say λ_1, has to be equal to zero in stationary processes to ensure the convergence of $\mathbf{P}^{(N)}(t)$ to equilibrium values, $\mathbf{P}^{(N)}(\infty)$. Furthermore, for processes where the principle of detailed balance applies as in the present case, all of the nonzero eigenvalues are strictly negative, rather than some of them being complex.[14] The product $\boldsymbol{B}^{(N)} \exp\{\boldsymbol{L}^{(N)}t\}[\boldsymbol{B}^{(N)}]^{-1}$ defines the conditional or transition probability matrix $\boldsymbol{C}^{(N)}(t)$. The ijth element $C_{ij}^{(N)}$ denotes the probability of occurrence of configuration $\{\phi\}_i$ at time t, for a sequence of N bonds in motion, given the initial configuration $\{\phi\}_j$. Here $\{\phi\}_i$, $i = 1, 3^N$, refers to a set of isomeric states characterizing a given configuration. Similarly the $3^N \times 3^N$ symmetric matrix $\boldsymbol{P}^{(N)}(t)$ is given by[1,5]

$$\boldsymbol{P}^{(N)}(t) = \boldsymbol{C}^{(N)}(t) \text{ diag } \mathbf{P}^{(N)}(0) \tag{5}$$

with

$$\boldsymbol{C}^{(N)}(t) = \boldsymbol{B}^{(N)} \exp\{\boldsymbol{L}^{(N)}t\}[\boldsymbol{B}^{(N)}]^{-1} \tag{6}$$

$\boldsymbol{P}^{(N)}(t)$ represents the joint probability matrix whose ijth element denotes the joint probability of occurrence of two configurations, $\{\phi\}_i$ and $\{\phi\}_j$, within a time interval t. $\boldsymbol{P}^{(N)}(t)$ or alternately $C^{(N)}(t)$ fully describes the conformational stochastics of the segment of N bonds subject to Brownian motion. In component form, eq 5 reads

$$P^{(N)}{}_{nk} = C^{(N)}{}_{nk}(t)P^{(N)}{}_k(0) \tag{7}$$

with

$$C^{(N)}{}_{nk}(t) = \sum B^{(N)}{}_{nj} \exp\{\lambda_j t\}[B^{(N)}{}_{jk}]^{-1} \tag{8}$$

The subscripts n and k index the elements that are associated with configurations $\{\phi\}_n$ and/or $\{\phi\}_k$.

Let us investigate the two limiting cases $t = 0$ and $t = \infty$, according to eq 7 and 8.

(i) When $t = 0$, eq 8 leads to

$$C^{(N)}{}_{nk}(0) = \delta_{nk} \tag{9}$$

as expected and consequently

$$P^{(N)}{}_{nk}(0) = \delta_{nk}P^{(N)}{}_k(0) \tag{10}$$

where δ_{nk} is the Kronecker delta.

(ii) As $t \to \infty$, all of the terms in eq 8 vanish (since λ_j's are negative) except for the one with the zero eigenvalue λ_1, such that

$$\begin{aligned} P^{(N)}{}_{nk}(\infty) &= C^{(N)}{}_{nk}(\infty)P^{(N)}{}_k(0) \\ &= B^{(N)}{}_{n1}[B^{(N)}{}_{1k}]^{-1}P^{(N)}{}_k(0) \end{aligned} \tag{11}$$

On the other hand, as $t \to \infty$, the events of occurrence of configurations $\{\phi\}_i$ and $\{\phi\}_j$ become independent; i.e.,

$$P^{(N)}{}_{nk}(\infty) = P^{(N)}{}_n(\infty)P^{(N)}{}_k(0) \tag{12}$$

or

$$C^{(N)}{}_{nk}(\infty) = P^{(N)}{}_n(\infty) \tag{13}$$

From the comparison of eq 11 and 12, it follows that the equilibrium probabilities may be found from the elements of $\boldsymbol{B}^{(N)}$ and $[\boldsymbol{B}^{(N)}]^{-1}$ associated with the zero eigenvalue λ_1, as

$$P^{(N)}{}_n(\infty) = B^{(N)}{}_{n1}[B^{(N)}{}_{1k}]^{-1} \tag{14}$$

It should be noted that $[B^{(N)}]_{1k}{}^{-1}$ is constant for all k; i.e., the subscript k is immaterial. Also, for stationary processes, if $\mathbf{P}^{(N)}(0)$ is set equal to $\mathbf{P}^{(N)}(\infty)$, the equilibrium distribution of configurations is conserved and hence $\mathbf{P}^{(N)}(t)$ is always given by the same column vector $\mathbf{P}^{(N)}(0)$ dictated by equilibrium statistics, regardless of the time argument. However, although the probability $\mathbf{P}^{(N)}(t)$ is independent of time, the joint probability $\boldsymbol{P}^{(N)}(t)$ of two different configurations for a given segment, with a time interval t, depends on t, inasmuch as the system is a dynamic one and any sequence is continuously subject to conformational transitions.

The elements of $\boldsymbol{P}^{(N)}(t)$ may be used as stochastic weights to determine the transient behavior of any configuration-dependent property. For instance, the OACF related to the initial and final orientations of a vector $\mathbf{m}$ rigidly embedded in the sequence in motion may be found from

$$M_1(t) = \langle \mathbf{m}(0)\cdot\mathbf{m}(t) \rangle \tag{15}$$

$$M_1(t) = \sum_i \sum_j \{P^{(N)}{}_{ij}(t)[\mathbf{m}_i\cdot\mathbf{m}_j]\} \tag{16}$$

and

$$M_2(t) = \langle 3/2[\mathbf{m}(0)\cdot\mathbf{m}(t)]^2 - 1/2 \rangle \tag{17}$$

$$M_2(t) = \sum_i \sum_j \{P^{(N)}{}_{ij}[3/2(\mathbf{m}_i\cdot\mathbf{m}_j)^2 - 1/2]\} \tag{18}$$

Here $M_1(t)$ and $M_2(t)$ are referred to as the first and second OACFs, respectively. The above equations may be generated for any property f_{ij} which is a function of the configurations $\{\phi\}_i$ and $\{\phi\}_j$. The ensemble average of f_{ij} over all possible conformational transitions is given by

$$\langle f_{ij} \rangle = \sum_i \sum_j P^{(N)}{}_{ij}(t)f_{ij} \tag{19}$$

$$\langle f_{ij} \rangle = \sum_{n=1}^{3^N} k_n \exp\{\lambda_n t\} \tag{20}$$

where

$$k_n = \sum_{j=1}^{3^N} \sum_{i=1}^{3^N} B^{(N)}{}_{in}[B^{(N)}{}_{nj}]^{-1}P^{(N)}{}_j(0)f_{ij} \tag{21}$$

Equations 20 and 21 directly follow from eq 7 and 8. Substitution of f_{ij} in eq 19–21 by $(\mathbf{m}_i\cdot\mathbf{m}_j)$, for example, yields $M_1(t)$, as apparent from eq 15 and 16. It should be noted that k_n depends on the molecular structure and the equilibrium statistics of the chain and on the specific quantity f_{ij} investigated. Thus, k_n is independent of time. All the time dependence of $\boldsymbol{P}^{(N)}(t)$ and consequently $\langle f_{ij}(t) \rangle$ is accounted for by the eigenvalues, as pointed out above.

Equations 20 and 21 offer a convenient form for transformation into the frequency domain. Accordingly, the spectral density function, which is the Fourier transform of the OACF, may be found from

$$J(\omega) = \int_0^\infty M_2(t) \exp\{i\omega t\} \, dt = -[\sum_{j=1}^{3^N} k_j\lambda_j/(\omega^2 + \lambda_j{}^2)] \tag{22}$$

The correlation time τ that characterizes the time scale for the decay of the autocorrelation function $M_i(t)$ ($i = 1$ or 2) is defined[15] by

$$\tau = \int_0^\infty [M_i(t) - M_i(\infty)][M_i(0) - M_i(\infty)]^{-1} \, dt \tag{23}$$

From eq 20, $M_i(t)$ may be written as a sum of exponentials; i.e.,

$$M_i(t) = \sum_{j=1}^{3^N} k_j \exp\{\lambda_j t\} \tag{24}$$

Scheme I

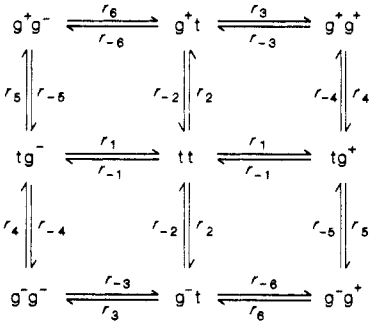

Initially $M_i(0) = 1$. At $t = \infty$, all of the terms in the summation vanish except for $k_1 \exp\{\lambda_1 t\}$, recalling that λ_1 is the zero eigenvalue. Thus, eq 23 becomes

$$\tau = \int_0^\infty [\sum_{j=2}^{3^N} k_j \exp(\lambda_j t)](1 - k_1)^{-1}\, dt = -(1 - k_1)^{-1} \sum_{j=2}^{3^N} (k_j/\lambda_j) \cong -[\sum_{j=2}^{3^N} k_j/\lambda_j] \quad (25)$$

The last equality holds if $k_1 \ll 1$.

Kinetics of Conformational Transitions in PEO. The kinetic scheme for conformational transitions in PEO ($-CH_2CH_2O-$) is different from the one proposed[1] for PE. In chains with identical skeletal bonds like PE, the states tg^+ and g^+t are indistinguishable from the point of view of prevailing configurational energy of interaction, since the same first-order interaction parameter applies to both adjacent bonds, whereas in PEO different energies are associated with those two states. The kinetic Scheme II of ref 1 is now replaced by Scheme I where r_i and r_{-i} (i = 1–6) are the rate constants corresponding to the indicated transitions. They are represented by Arrhenius-type expressions, with activation energies or energy barriers $E_{a,i}$ deduced from the heights of the saddles between isomeric minima in the two-dimensional conformational maps, as

$$r_i = A_0 \exp\{-E_{a,i}/RT\} \quad (26)$$

where R is the gas constant and T is the absolute temperature. The front factor A_0 is given by

$$A_0 = (\gamma\gamma^*)^{1/2}/2\pi\zeta \quad (27)$$

following Kramers' expression[16] for high friction medium. Here ζ is the friction coefficient, γ and γ^* are the force constants associated with the shape of the potential wells and barriers, respectively. In view of the lack of detailed information on those parameters, the front factor will be kept as a constant for all conformational transitions. A similar approach is commonly used in the equilibrium statistics[17] of macromolecules, where the shape of the energy minima is not considered, except for a few refined treatments. By use of Stoke's law for the friction coefficient, A_0 is assumed to be inversely proportional to solvent viscosity, as a first-order approximation.

As may be seen from the above kinetic scheme, the allowable transitions involve rotations of either the left or the right bonds of the pair. Accordingly, $\mathbf{A}^{(2)}_{j,j+1}$ in eq 2 may be decomposed into two components, $\mathbf{A}_L$ and $\mathbf{A}_R$, representing the transition rate matrices of the left and right bonds of the pair, respectively. $\mathbf{A}_L$ and $\mathbf{A}_R$ are given by Charts I and II. By the use of $\mathbf{A}_L$ and $\mathbf{A}_R$, $\mathbf{A}^{(2)}_{j,j+1}$ may be expressed as

$$\mathbf{A}^{(2)}_{i,i+1} = \begin{cases} \mathbf{A}_L + \mathbf{A}_R/2 & i = 1 \\ {}^1/_2[\mathbf{A}_L + \mathbf{A}_R] & 1 < i < N-1 \\ \mathbf{A}_L/2 + \mathbf{A}_R & i = N-1 \end{cases} \quad (28)$$

Chart I

$$\mathbf{A}_L = \begin{bmatrix} -2r_2 & 0 & 0 & r_{-2} & 0 & 0 & r_{-2} & 0 & 0 \\ 0 & -r_{-4}-r_5 & 0 & 0 & r_4 & 0 & 0 & r_{-5} & 0 \\ 0 & 0 & -r_5-r_{-4} & 0 & 0 & r_{-5} & 0 & 0 & r_{-4} \\ r_2 & 0 & 0 & -r_{-2} & 0 & 0 & 0 & 0 & 0 \\ 0 & r_{-4} & 0 & 0 & -r_4 & 0 & 0 & 0 & 0 \\ 0 & 0 & r_5 & 0 & 0 & -r_{-5} & 0 & 0 & 0 \\ r_2 & 0 & 0 & 0 & 0 & 0 & -r_{-2} & 0 & 0 \\ 0 & r_5 & 0 & 0 & 0 & 0 & 0 & -r_{-5} & 0 \\ 0 & 0 & r_{-4} & 0 & 0 & 0 & 0 & 0 & -r_{-4} \end{bmatrix}$$

Chart II

$$\mathbf{A}_R = \begin{bmatrix} -2r_1 & r_{-1} & r_{-1} & 0 & 0 & 0 & 0 & 0 & 0 \\ r_1 & -r_{-1} & 0 & 0 & 0 & 0 & 0 & 0 & 0 \\ r_1 & 0 & -r_{-1} & 0 & 0 & 0 & 0 & 0 & 0 \\ 0 & 0 & 0 & -r_{-6}-r_3 & r_{-3} & r_6 & 0 & 0 & 0 \\ 0 & 0 & 0 & r_3 & -r_{-3} & 0 & 0 & 0 & 0 \\ 0 & 0 & 0 & r_{-6} & 0 & -r_6 & 0 & 0 & 0 \\ 0 & 0 & 0 & 0 & 0 & 0 & -r_{-6}-r_3 & r_6 & r_{-3} \\ 0 & 0 & 0 & 0 & 0 & 0 & r_{-6} & -r_6 & 0 \\ 0 & 0 & 0 & 0 & 0 & 0 & r_3 & 0 & -r_{-3} \end{bmatrix}$$

By introducing the factor ${}^1/_2$ in eq 28, a representative average rate is adopted for the rotation of a given bond i which is simultaneously a member of the pairs $(i-1,i)$ and $(i,i+1)$. The present, more rigorous formulation of $\mathbf{A}^{(2)}_{j,j+1}$ replaces the one given in ref 1. As usual, the diagonal elements in $\mathbf{A}^{(2)}_{j,j+1}$ are negative, and the elements in each column sum up to unity. It should be noted that, for PEO, the transition rate matrix assumes three distinct values depending on the pair of skeletal bonds, (OC,CC), (CC,CO) or (CO,OC).

For symmetric chains with identical skeletal bonds such as PE, we have $r_{\pm 1} = r_{\pm 2}$, $r_{\pm 3} = r_{\mp 4}$, $r_{\pm 5} = r_{\mp 6}$ such that $\mathbf{A}_L + \mathbf{A}_R$ reduces to the transition rate matrix introduced in ref 1. If, furthermore, bonds are assumed to be independent, we have $r_{\pm 1} = r_{\pm 2} = r_{\pm 3} = r_{\mp 4} = r_{\pm 5} = r_{\mp 6}$. In this case the transition rate matrix for single bonds is given by[5]

$$\mathbf{A}^{(1)} = \begin{bmatrix} -2r_1 & r_{-1} & r_{-1} \\ r_1 & -r_{-1} & 0 \\ r_1 & 0 & -r_{-1} \end{bmatrix} \quad (29)$$

and $\mathbf{A}_L$ and $\mathbf{A}_R$ equate to

$$\mathbf{A}_L = \mathbf{A}^{(1)} \otimes \mathbf{I}_3$$
$$\mathbf{A}_R = \mathbf{I}_3 \otimes \mathbf{A}^{(1)} \quad (30)$$

in agreement with Jernigan's treatment.[5]

III. Calculations

The size of the matrix to be diagonalized and inverted limits the application of the present analysis to relatively short sequences. In the present study, the motion of the terminal bond-based frame[1,4] in a sequence of six bonds in PEO is analyzed, for illustrative purposes. The absolute location and orientation of the sequence being immaterial, the first two bonds are assumed to be fixed in space, and a total of $3^4 = 81$ configurations (i.e., 81 eigenvalues) and hence $3^8 = 6561$ transitions are considered. It is worth noting that the choice of four mobile bonds is sufficient to represent the dynamic features of the three different bond pairs (OC,CC), (CC,CO), and (CO,OC). The energy parameters for the isomeric minima and the barrier heights in PEO are estimated from the works of Flory and collaborators[18-21] and Abe et al.[22] and also from conformational energy calculations carried out in the present study following the usual semiempirical methods. Let $E_{\sigma,i}$ denote the first neighbors interaction parameter for bond i and $E_{\omega,i}$ the one associated with second neighbors interactions for the pair of bonds i and $i-1$. Assuming the second-

Table I
Parameters for Energy Minima (Kilocalories/Mole)

bond	$E_{\sigma;i}$	$E_{\omega;i}$
CO	0.90	0.34
OC	0.90	8.10
CC	−0.43	0.34

Table II
Heights of Saddles (Kilocalories/Mole) with Respect to tt Minima

between	(CC,CO)	(CO,OC)	(OC,CC)
$tt \leftrightarrow tg^{\pm}$	2.7	2.7	3.5
$tt \leftrightarrow g^{\pm}t$	3.5	2.7	2.7
$g^{\pm}t \leftrightarrow g^{\pm}g^{\pm}$	2.3	3.4	3.7
$g^{\pm}g^{\pm} \leftrightarrow tg^{\pm}$	3.7	3.4	2.3
$tg^{\pm} \leftrightarrow g^{\mp}g^{\pm}$	3.7	12	2.3
$g^{\mp}g^{\pm} \leftrightarrow g^{\mp}t$	2.3	12	3.7

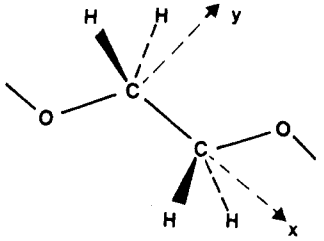

Figure 1. Portion of a mobile sequence and a coordinate system affixed to the CC bond.

order interactions to be operative only in the case of pentane effect (i.e., $g^{\pm}g^{\mp}$ state), the energy minima in the two-dimensional energy maps are

$$E(tt) = 0$$

$$E(tg^{\pm}) = E_{\sigma;i}$$

$$E(g^{\pm}t) = E_{\sigma;i-1}$$

$$E(g^{\pm}g^{\pm}) = E_{\sigma;i} + E_{\sigma;i-1}$$

$$E(g^{\pm}g^{\pm}) = E_{\sigma;i} + E_{\sigma;i-1} + E_{\omega;i} \qquad (31)$$

The energy parameters adopted in the present study are listed in Table I, for the three types of skeletal bonds in PEO. The activation energies for various conformational transitions, estimated from the heights of the saddles in conformational maps, are listed in Table II. The $g^{\pm}g^{\mp}$ state for the (CO,OC) pair is highly unfavorable from an energetic point of view and is neglected in equilibrium calculations. Accordingly, a high activation energy ($\simeq$12 kcal/mol) practically forbidding the passage to that state has been adopted.

The transition rate matrices $\mathbf{A}^{(2)}_{j,j+1}$ defined by Charts I and II and eq 28 are inserted into eq 2 to determine the rate matrix $\mathbf{A}^{(N)}$ governing the kinetics of the sequence of $N = 4$ bonds. $\mathbf{A}^{(N)}$ is transformed following eq 4 to evaluate $\boldsymbol{B}^{(N)}$ and $\boldsymbol{L}^{(N)}$ whose elements are subsequently used in eq 20 and 21 to obtain the ensemble averaged time dependence of the property f_{ij}. The spectral density and the correlation time associated with f_{ij} are readily found from eq 22 and 25, respectively.

Orientational Autocorrelation Functions. Figure 1 represents a portion of a PEO chain. For illustrative purposes a local coordinate system is shown, with the x axis along the C–C bond. The y axis lies in the plane of the figure and is chosen so as to make an acute angle with the extension of the preceding bond. The z axis completing a right-handed coordinate system is not shown in the figure.

The orientational autocorrelation function $M_{2x}(t)$ for a vector along skeletal bonds, i.e., the x axis of the local frame in motion, in PEO at 300 K is shown in Figure 2. Equations 21 and 24 with $f_{ij} = [3(\mathbf{m}_i \cdot \mathbf{m}_j)^2 - 1]/2$ have been used in calculations.

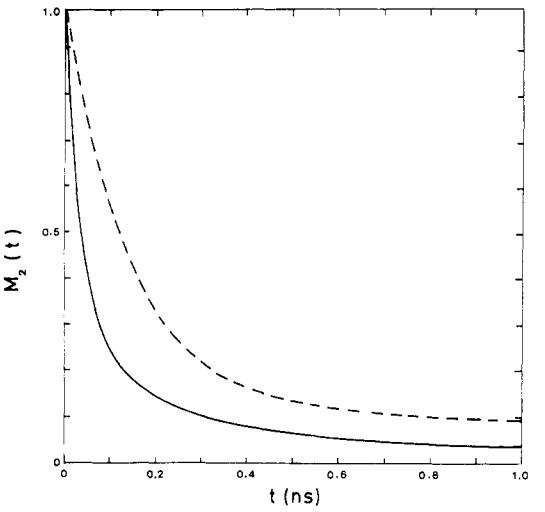

Figure 2. Decay with time of the second OACF for the Nth bond vector from a fixed end in PEO (solid curve) and PE (dashed curve) chains, with $N = 6$, $T = 300$ K, and $A_0 = 2.77 \times 10^{11}$ s^{-1}. Data from Table I and II have been used for PEO.

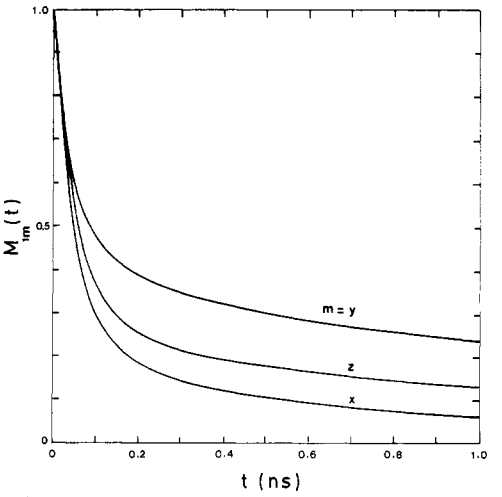

Figure 3. Decay of the first OACFs $M_{1m}(t)$ with time for **m** = **x**, **y**, and **z** in the local frame in motion. The curves are calculated for PEO, with the same data as in Figure 1.

For comparison, the equivalent curve obtained for PE with the same front factor, $\mathbf{A}_0 = 2.77 \times 10^{11}$/s as the one adopted in previous studies,[1-4] is given by the dashed curve. It is clearly seen that PEO relaxes much faster than PE, as expected from their conformational characteristics. In fact, the energy barriers in PEO are in general lower than those in PE.

Figure 3 displays the decay of the first OACF $M_{1m}(t)$ with time, for PEO. The curves are drawn for the three axial vectors **m** = **x**, **y**, and **z** spanning the local frame in motion. Calculations are performed with the same data as those for Figure 2. It is interesting to note that vectors along skeletal bonds are those which relax the fastest. This behavior is in contrast to the one calculated[3,4] for PE, where the OACF of bond vectors decays slower compared to those for vectors along y and z. This feature is a direct consequence of the drastic differences between the conformational characteristics of PE and PEO chains. In PEO, gauche states are more favorable from an energy point of view, leading to a loss of orientation for vectors along the backbone, while in PE, the most probable state being the trans state, there is higher persistence along the

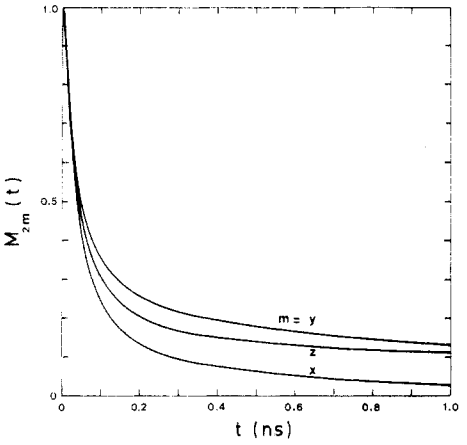

Figure 4. Decay of the second OACF $M_{2m}(t)$. See legend for Figure 3.

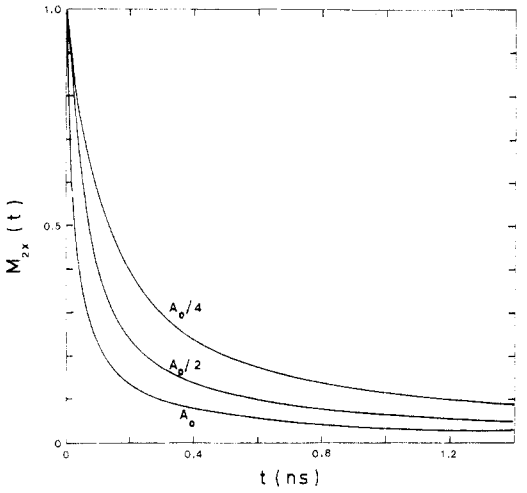

Figure 5. Effect of solvent viscosity on OACFs for PEO. The lower curve is identical with the one in Figure 2. The two upper curves are obtained using the front factors $A_0/2$ and $A_0/4$ to account for the effect of doubling the viscosity, all of the other parameters being unchanged. The relaxation times are found to be linearly proportional to solvent viscosity.

x direction. Calculations performed for the second OACFs indicate that similar behavior is valid for the second OACFs, as shown in Figure 4.

It should be noted that the OACFs in Figures 2–5 do not decay to zero. In fact, in the limit as $t \rightarrow \infty$, all the exponentials contributing to $\mathbf{M}_i(t) = \sum k_j \exp\{\lambda_j t\}$ vanish, except for the one corresponding to the zero eigenvalue λ_1, i.e., $M_i(\infty) = k_1$, a value which is determined by the specific characteristics of the chain. For the curves in Figure 3, k_1 (or $M_{1m}(\infty)$) equals 8.8×10^{-3}, 0.13, and 3.2×10^{-4} for **m** = **x**, **y**, and **z**. Similarly the respective asymptotic values in Figure 4 are 5.9×10^{-3}, 6.4×10^{-2}, and 7.4×10^{-2}. Full relaxation takes place only if an overall rotation is superimposed, i.e., the first bond of the sequence is allowed to undergo orientational motion. However, the contribution of the relatively slow overall motion to the predicted OACFs is expected to be negligibly small in the range $t < 1$ ns.

To show the influence of the effective viscosity, η, on the relaxation behavior, a series of $M_{2x}(t)$ curves obtained by modifying the front factor, A_0, are drawn in Figure 5. From the analysis of the k_j and λ_j values corresponding to different viscosities, it is observed that the doubling of the front factor, A_0 (or halving of η), is directly reflected upon the eigenvalues which are equally doubled while k_j values remain unchanged. This is in conformity with the definition of k_j's above, where it is asserted that they are determined by the equilibrium statistics of the investigated property and only the eigenvalues account for any time dependence.

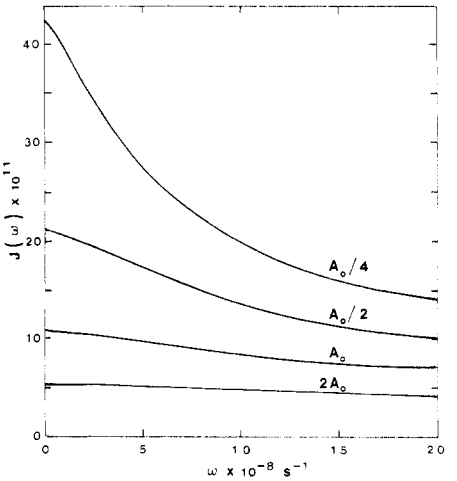

Figure 6. Frequency dependence of spectral density function for the sixth bond from a fixed origin in PEO, at 35 °C. The curves represent $J(\omega)$ for various solvent viscosities which are assumed to be inversely proportional to the front factors (A_0, $2A_0$, etc.) in the rate expressions. The intercept represents the corresponding correlation times. $A_0 = 2.77 \times 10^{11}$ s^{-1}.

Spectral Density Functions. Figure 6 displays the spectral density functions $J(\omega)$ associated with $M_{2x}(t)$, i.e., calculated from eq 22 with the k_j values corresponding to the second OACF of the Nth bond vector in PEO, with $N = 6$, $T = 35$ °C. As the shape of $J(\omega)$ depends on the value of the front factor, A_0, as an illustration, the spectral density functions are drawn for four different front factors, $A_0/4$, $A_0/2$, A_0, and $2A_0$, choosing $A_0 = 2.77 \times 10^{11}$/s as above and keeping all of the other parameters constant. Clearly, the change in the front factor from $A_0/4$ to $2A_0$ is equivalent to a decrease in viscosity by a factor of 8, following the approximation of the inverse proportionality between A_0 and η, as mentioned above. The highest frequency dependence, in the range $0 < \omega < 2 \times 10^8$/s, is exhibited by the chain with the lowest front factor, i.e., in a solvent with relatively high viscosity. The frequency dependence is weaker in media allowing for fast motions, as the extreme narrowing limit is approached. At the intercept, $J(0)$ becomes identically equal to the correlation time, τ, as apparent from eq 22 and 25.

Frequency Distribution of Relaxational Modes. From eq 24, it clearly appears that λ_n represents the frequency of the nth mode of relaxation and k_n is the corresponding a priori probability of relaxation through mode n. In fact, for the case when $\langle f_{ij}(t) \rangle$ represents the OACFs associated with unit vectors **m**, we have $\sum k_n = 1$. Thus, k_n values characterize the distribution of relaxational modes. Inasmuch as k_n depends on the property investigated, different frequency distribution curves are obtained for different directions. For illustrative purposes, the frequency distribution of the relaxational modes associated with the second OACF for a vector along the C–H bonds in PEO, at 300 K, is shown in Figure 7. Data from Tables I and II have been used in the calculations. The abscissa in the figure (log $(-\lambda_n)$, λ_n in s^{-1}) has been divided into intervals of 0.5, in the range $8.5 < \log(-\lambda_n) < 11$. The ordinate represents the sum of the a priori probabilities in each interval. The number of relaxational modes and the corresponding probabilities, $\sum k_n$, in each interval are listed in Table III. It is interesting to note that the frequency distribution is rather large (it covers 2 decades) and

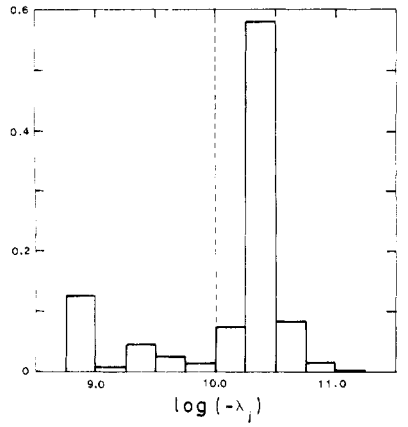

Figure 7. Distribution of frequencies of various relaxational modes for ^{13}C NMR at 27 °C. $A_0 = 2.77 \times 10^{11}$ s^{-1}. The vertical dashed line indicates the lower cutoff for frequencies used in the calculations.

Table III
Data for Figure 7

interval of log (-λ)	no. of eigenvalues in the interval	$\sum k_j$ in each interval[a]
8.75–9.00	2	0.1258
9.00–9.25	1	0.0063
9.25–9.50	2	0.0459
9.50–9.75	2	0.0229
9.75–10.00	1	0.0156
10.00–10.25	8	0.0774
10.25–10.50	28	0.5807
10.50–10.75	18	0.0811
10.75–11.00	18	0.0172

[a] $k_1 = 0.0271$ for the zero eigenvalue.

two peaks centered at about log $(-\lambda_n) = 8.9$ and 10.4 are obtained. Calculations show that same qualitative features are preserved for different temperatures and directions of **m**.

IV. Comparison with Experiments

In the following, the predictions of the theory are compared with the correlation times and spin–lattice relaxation times measured in the ^{13}C NMR and ^1H NMR experiments.

With the assumption of a purely ^{13}C–^1H dipolar relaxation mechanism, the spin–lattice relaxation time, T_{1C}, in the ^{13}C NMR experiments is given by[23]

$$1/T_{1C} = [n_0\hbar^2\gamma_C^2\gamma_H^2/10r_{CH}^6] \times [J(\omega_H - \omega_C) + 3J(\omega_C) + 6J(\omega_H + \omega_C)] \quad (32)$$

where $\hbar = h/2\pi$, h is the Planck's constant, γ_H and γ_C are the gyromagnetic ratios, and ω_H and ω_C are the resonance frequencies of the hydrogen and carbon nuclei, respectively. r_{CH} is the internuclear distance, which is taken to be equal to 1.1 Å in the calculations. n_0 denotes the number of protons (here 2) contributing to the dipolar interaction with the ^{13}C nucleus.

As to the spin–lattice relaxation time, T_{1H}, measured in ^1H NMR, it is given[24] by

$$1/T_{1H} = [3\hbar^2\gamma_H^4/10r_{HH}^6][J(\omega_H) + 4J(2\omega_H)] \quad (33)$$

assuming a purely ^1H–^1H dipolar relaxation mechanism between proton pairs. Here r_{HH} is the distance between the interacting protons. For PEO, the internuclear separation, r_{HH}, is taken as 1.8 Å.

It should be noted that the spectral density functions, $J(\omega)$, which are used in eq 32 and 33 differ from each other inasmuch as they are calculated for specific internuclear vectors with different orientations with respect to the backbone. In fact, the unit vector **m** involved in ^1H NMR is along the z axis of the local frame (Figure 1), while **m** in ^{13}C NMR, which is identical with the C–H bond vector, is a combination of the three axial directions and is calculated using the geometrical parameters of PEO. The resulting k_j values and consequently the spectral densities will be different for the two types of experiments. Similarly, distinct correlation times τ_C and τ_H are associated with ^{13}C and ^1H NMR, respectively. The frequency dependence of $J(\omega)$ is expected to vanish in media, allowing for relatively fast motions, such that $\lambda_j \gg (\omega_H + \omega_C)$, for all j. Measurements carried out under such extreme narrowing limit conditions may be used to calculate the prevailing correlation times, referred to as the isotropic correlation times, according to

$$1/T_{1C} = n_0\hbar^2\gamma_C^2\gamma_H^2\tau_C/r_{CH}^6 \quad (34)$$

and

$$1/T_{1H} = 3\gamma_H^4\hbar^2\tau_H/r_{HH}^6 \quad (35)$$

Equations 34 and 35 directly follow from eq 32 and 33, respectively, in which the spectral density functions reduce to the isotropic correlation times, $\tau = \sum_{j=2}^{3} k_j/\lambda_j$, regardless of the frequency argument. Subscripts C and H appended to τ refer to ^{13}C and ^1H NMR, respectively.

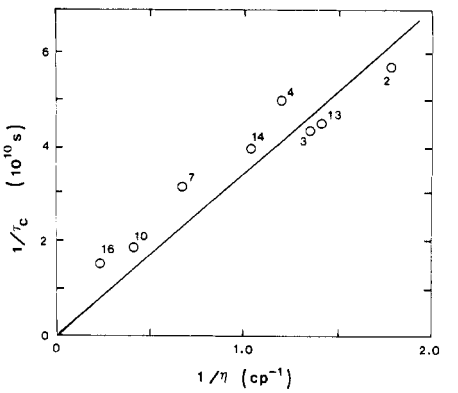

Figure 8. Isotropic correlation times τ_C from ^{13}C NMR as a function of solvent viscosity for dilute PEO solutions in the various solvents listed in Table III. Empty circles result from the experiments of Lang et al.[12] at 30 °C. The solid line is calculated by the dynamic RIS model with the data in Tables I and II, using eq 21 and 25 where $\langle f_{nk} \rangle = M_{2m}(t)$; **m** is the C–H bond vector. $A_0 = 2.77 \times 10^{11}/\eta$ where A_0 is in s^{-1} and η is in cP. The same conformational data and front factor are used in Figures 9–11.

The results from the ^{13}C NMR experiments by Lang et al.[12] on dilute PEO solutions are shown in Figure 8. Experiments are performed at 30 °C and 25.2 MHz in various solvents. Only those solvents not leading to hydrogen bonding with PEO are included in the figure. The experimental correlation times are presented as a function of solvent viscosity. Similarly, Figures 9 and 10 display the results from ^1H NMR at 35 °C and 50 MHz. Experimental points from the work of Liu and Anderson[10] are shown by the empty circles. Diamonds represent the measurements by Hermann and Weill[11] for PEO in p-chlorophenol at various temperatures.

The small numbers next to the experimental points in Figures 8–10 refer to the solvents listed in Table IV. The experimental data are reported in both cases to be obtained under extreme narrowing limit conditions; i.e., the dependence on the operating frequency is negligibly small. This indicates that only those eigenvalues $\lambda_n \gg (\omega_H + \omega_c)$ are operative. We consider accordingly a range of relaxational frequencies corresponding to relatively fast mot-

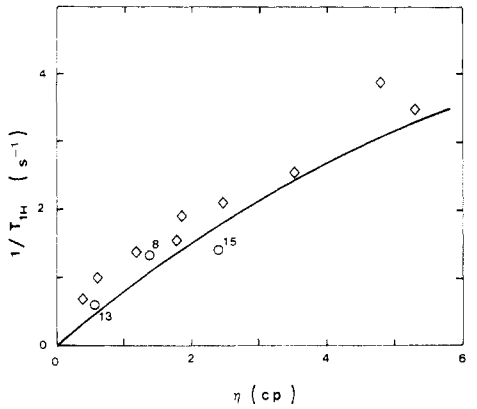

Figure 9. Spin–lattice relaxation times T_{1H} for PEO from ^1H NMR as a function of solvent viscosity at 35 °C. Circles and diamonds represent the experimental results from ref 10 and 11, respectively. The solid curve is calculated by the dynamic RIS model for 50.0 MHz, $\mathbf{m} = \mathbf{z}$, using eq 21, 22, and 33.

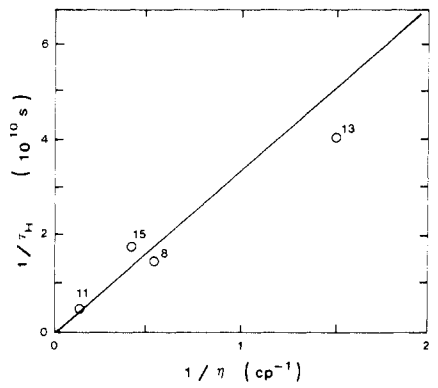

Figure 10. Isotropic correlation times τ_H from ^1H NMR, as a function of solvent viscosity, at 35 °C for dilute PEO solutions with the solvents listed in Table III. Empty circles are calculated[12] from the spin–lattice relaxation times measured by Liu and Anderson[10] at 50 MHz, assuming extreme narrowing limit conditions. The solid line is calculated by the dynamic RIS model.

Table IV
Solvents in NMR Experiments[a]

3, CH_2ClCH_2Cl	10, CH_2I_2
4, CCl_4	13, chlorobenzene
7, CH_2BrCH_2Br	15, α-chloronaphthalene
8, $CHCl_2CCl_3$	16, α-bromonaphthalene

[a] Same indexes as those in ref 12 are assigned to the solvents.

ions. This is established through introduction of a suitable cutoff in the frequency distribution function in Figure 7. The vertical dashed line in the figure indicates the cutoff introduced in the present calculations. Relaxation modes lying in the left-hand side of the cutoff are omitted in the calculations. This region corresponds to modes with relaxation times which are at least 1 order of magnitude larger than the observed correlation times (see sequel) such that their superposition on the observed faster modes is inconsequential.

As mentioned above, the k_j values in the dynamic RIS model are inherently determined by the chemical structure and equilibrium statistics of the chain and are calculated for the specific property f_{nk} investigated according to eq 21. Here $f_{nk} = [3(\mathbf{m}_n \cdot \mathbf{m}_k)^2 - 1]/2$, where $\mathbf{m}$ is replaced by suitable internuclear vectors. In the local bond-based coordinate system,[1,17] $\mathbf{m}$ equates to the column vectors $(0\ 0\ 1)^T$ for ^1H NMR and $(-0.323\ \ 0.479\ \ 0.817)^T$ for ^{13}C NMR, as follows from the molecular geometry of PEO. The dynamic behavior of the chain is dictated by the eigenvalues, λ_j. The calculations in section III demonstrated

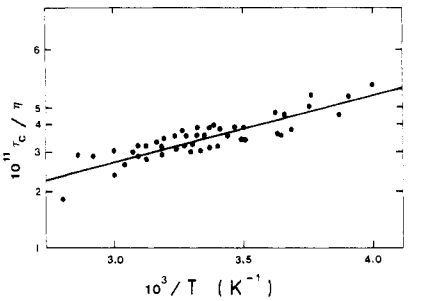

Figure 11. Temperature dependence of correlation times. Points represent experimental data from ref 12. The solid line is obtained by the present theory, leading to an activation energy of 1.8 kcal/mol.

that λ_j's are linearly proportional to the front factor, A_0 in the rates r_i (or r_{-i}) between conformers; i.e.,

$$|\lambda_j| \sim A_0 \qquad j = 1, 3^N \tag{36}$$

But from eq 27, $A_0 \sim \zeta^{-1}$, or using Stoke's law we have

$$A_0 \sim \eta^{-1} \tag{37}$$

Combining the proportionalities given by eq 36 and 37, we end up with

$$|\lambda_j| \sim \eta^{-1} \qquad j = 1, 3^N \tag{38}$$

or from eq 27,

$$1/\tau \sim 1/\eta \tag{39}$$

The results from calculations are shown by the curves in Figures 8–10. Calculations are performed with the data in Tables I and II, and the front factor $A_0 = [2.77 \times 10^{11}/\eta]$ s^{-1}, where η is in centipoises. The latter is found to yield the best agreement with ^{13}C NMR and ^1H NMR and electron spin resonance (ESR) (Figure 11) experiments, simultaneously. It is interesting to note that, from the ESR study of dilute PEO solutions at different temperatures, Friedrich et al.[25] estimate a relationship between A_0 and η^{-1} of the form $A_0 = [3.03 \times 10^{11}/\eta]$ s^{-1}, which is in close agreement with the normalization of A_0 adopted in the present study.

The dependence of correlation times on temperature is displayed by the Arrhenius plot in Figure 11. Points represent experimental data from the work of Friedrich et al.[25] The solid line is theoretically obtained by repeating the above calculations for various temperatures. The lines obtained for τ_C and τ_H are indistinguishable on a logarithmic scale. The same activation energy, equal to 1.8 kcal/mol, is theoretically obtained both for ^1H NMR and ^{13}C NMR, confirming that energies of about one barrier height between isomeric states activate local conformational transitions in polymeric chains in dilute solution. The relatively low apparent activation energy (compared to those listed in Table II) mainly originates from the frequency cutoff adopted in the theoretical spectrum of relaxational modes.

V. Conclusions

The present analysis leads to the following concluding remarks:

(1) The stochastics of conformational transitions in a given polymer in dilute solution are governed by a set of eigenvalues λ_j that are found from the solution of the master equation describing the motion of a short sequence. Their absolute values may be identified as the frequencies of individual modes contributing to relaxation on a local scale. They are characteristic of a given chain at a given temperature and are linearly proportional to $1/\eta$.

(2) Properties such as OACFs, correlation times, and spectral densities are easily calculated using λ_j's together with the weighting factor k_j's, which equally follow from the master equation but assume different values depending on the property investigated and the equilibrium statistics of the chain.

(3) Local chain dynamics is found to be significantly dependent upon the molecular structure, as the comparison of OACFs for PE and PEO in Figure 1 indicates.

(4) The present form of the dynamic RIS model which is developed for relatively short sequences in motion seems suitable for the interpretation of high-frequency motions of the order 10^{10}–10^{11}/s and, in particular, the spin–lattice relaxation and correlation times measured in NMR experiments with dilute polymeric solutions. The theory satisfactorily reproduces the experimentally measured spin–lattice relaxation and correlation times in ^1H and ^{13}C NMR, as well as the observed activation energies and the front factor, A_0. The agreement of the latter lends support to the postulated inverse linear dependence of A_0 on viscosity.

Acknowledgment. Financial support by NATO Grant 0321/87 is gratefully acknowledged. The authors thank Dr. F. Laupretre for useful discussions.

Registry No. PEO, 25322-68-3.

References and Notes

(1) Bahar, I.; Erman, B. *Macromolecules* **1987**, *20*, 1369.
(2) Bahar, I.; Erman, B. *Macromolecules* **1987**, *20*, 2310.
(3) Bahar, I.; Erman, B. *J. Chem. Phys.* **1988**, *88*, 1228.
(4) Bahar, I.; Erman, B.; Monnerie, L. *Macromolecules* **1989**, *22*, 431. Bahar, I.; Erman, B.; Monnerie, L. *Polym. Commun.* **1988**, *29*, 349.
(5) Jernigan, R. L. In *Dielectric Properties of Polymers*; Karasz, F. E., Ed.; Plenum: New York, 1972; p 99.
(6) Weber, T. A.; Helfand, E. *J. Phys. Chem.* **1983**, *87*, 2881.
(7) Hall, C.; Helfand, E. *J. Chem. Phys.* **1982**, *77*, 3275.
(8) Bendler, J. T.; Yaris, R. *Macromolecules*, **1978**, *11*, 650.
(9) Matsuo, K.; Stockmayer, W. H. *J. Phys. Chem.* **1983**, *87*, 2911.
(10) Liu, K. J.; Anderson, J. E. *Macromolecules* **1970**, *3*, 163.
(11) Hermann, G.; Weill, G. *Macromolecules* **1975**, *8*, 171.
(12) Lang, M.-C.; Laupretre, F.; Noel, C.; Monnerie, L. *J. Chem. Soc., Faraday Trans. 2* **1979**, *75*, 349.
(13) Heatley, F.; Walton, I. I. *Polymer* **1976**, *17*, 1019.
(14) Oppenheim, I.; Shuler, G. H.; Weiss, G. H. *Adv. Mol. Relax. Processes* **1967**, *1*, 13.
(15) Berne, B. J.; Pecora, R. *Dynamic Light Scattering*; Wiley: New York, 1976.
(16) Kramers, H. A. *Physica (Amsterdam)* **1940**, *7*, 284.
(17) Flory, P. J. *Statistical Mechanics of Chain Molecules*; Interscience: New York, 1969.
(18) Flory, P. J.; Mark, J. E. *Makromol. Chem.* **1964**, *75*, 11.
(19) Mark, J. E.; Flory, P. J. *J. Am. Chem. Soc.* **1966**, *87*, 1415.
(20) Mark, J. E.; Flory, P. J. *J. Am. Chem. Soc.* **1966**, *88*, 3702.
(21) Abe, A.; Kennedy, J. W.; Flory, P. J. *J. Polym. Sci., Polym. Phys. Ed.* **1976**, *14*, 1337.
(22) Abe, A.; Tasaki, K.; Mark, J. E. *Polym. J. (Tokyo)* **1985**, *17*, 883. Tasaki, K.; Abe, A. *Polym. J. (Tokyo)* **1985**, *17*, 641.
(23) Allerhand, A.; Doddrell, D.; Komoroski, R. J. *J. Chem. Phys.* **1971**, *55*, 189.
(24) Abragam, A. *Principles of Nuclear Magnetism*; Oxford University Press: London, 1961.
(25) Friedrich, C.; Laupretre, F.; Noel, C.; Monnerie, L. *Macromolecules* **1980**, *13*, 1625.
(26) Hermann, G. These d'Etat, Strasbourg, 1973 (from ref 25).
(27) Braun, D.; Tormala, P. *Makromol. Chem.* **1978**, *179*, 1025.

Polymeric Micelles: Their Relaxation Kinetics

A. Halperin*

The Fritz Haber Research Center for Molecular Dynamics, The Hebrew University, Jerusalem 91904, Israel, and Materials Department, University of California, Santa Barbara, California 93106

S. Alexander

Racah Institute of Physics, The Hebrew University, Jerusalem 91904, Israel.
Received July 27, 1988; Revised Manuscript Received October 19, 1988

ABSTRACT: Relaxation experiments—such as T jump—in solutions of polymeric micelles are theoretically analyzed. Only micelles formed by neutral A–B diblock copolymers in a selective solvent of low molecular weight are considered. The Aniansson–Wall mechanism, which allows the micellar size distribution to adjust in steps consisting of single-chain insertion/expulsion, is found to have the lowest activation free energy. The relaxation behavior is expected, as usual for micellar solutions, to be characterized by two relaxation times. The scaling form of the fast relaxation time, τ_1, is obtained by use of the properly adapted Kramers rate theory. τ_1 is found to have different forms for starlike micelles and for micelles with thin coronas. In both cases, $\tau_1 \sim \exp(N_B^{2/3}\gamma a^2/kT)$ where N_B is the core block's degree of polymerization (DP) and γ the surface tension of the core–corona interface. The preexponential factor is, however, different in the two systems. In solutions well past the critical micelle concentration (cmc), the preexponential factor scales as $N_B^{7/3}$ for micelles with thin coronas ($N_B \gg N_A$) and as $N_A^{9/5}N_B^{22/5}$ for starlike micelles ($N_B \ll N_A$) where N_A is the coronal block's DP. The different scaling laws are obtained because the passage through the corona is the rate-determining step only in starlike micelles.

I. Introduction

Much attention was given to the kinetics of micelle formation and dissolution.[1,2] Both experiment and theory focused on the response of micellar solutions to small perturbations, that is, relaxation experiments such as T jump. Most investigations dealt with the behavior of micelles formed by ordinary, small surfactants ($\sim C_{20}$). Very little, however, is known of the kinetics of polymeric micelles,[3] i.e., micelles formed by polymeric surfactants such as diblock copolymers. Studies of polymeric micelles, experimental[3,4] as well as theoretical,[5–11] considered their equilibrium properties. Yet, the kinetics of polymeric micelles should prove of interest both from polymer and

* Presently at The Hebrew University.

0024-9297/89/2222-2403$01.50/0